Chapter 4

Enhancement of Perfluorooctanoate (PFOA) and Perfluorooctanesulfonate (PFOS) Activity at Acoustic Cavitation Bubble Interfaces

Sections reprinted with permission from Vecitis C. D.; Park H.; Cheng J.; Mader, B. T.; Hoffmann, M. R.; J*ournal of Physical Chemistry C* **2008**, *112*, 16850–16857.

Abstract

Acoustic cavitation driven by ultrasonic irradiation decomposes and mineralizes the recalcitrant perfluorinated surfactants, perfluorooctanesulfonate (PFOS) and perfluorooctanoate (PFOA). Pyrolytic cleavage of the ionic headgroup is the rate-determining step. In this study, we examine the sonochemical adsorption of PFOX, where X = S for PFOS and A for PFOA, by determining kinetic order and absolute rates over an initial PFOX concentration range of 20 nM to 200 μM. Sonochemical PFOX kinetics transition from pseudo-first-order at low initial concentrations, $[PFOX]_i$ < 20 μM, to zero-order kinetics at high initial concentrations, $[PFOX]_i$ > 40 μM, as the bubble interface sites are saturated. At PFOX concentrations below 100 μM, concentration-dependent rates were modeled with Langmuir-Hinshelwood kinetics. Empirically determined rate maximums, V_{Max}^{-PFOA} = 2230 ± 560 nM min^{-1} and V_{Max}^{-PFOS} = 230 ± 60 nM min^{-1}, were used in the LH model, and sonochemical surface activities were estimated to be, K_{Sono}^{PFOS} = 120,000 M^{-1} and K_{Sono}^{PFOA} = 28,500 M^{-1}—60 and 80 times greater than equilibrium surface activities, K_{Eq}^{PFOS} and K_{Eq}^{PFOA}. These results suggest enhanced sonochemical degradation rates for PFOX when the bubble interface is under-saturated populated. The present results are compared to previously reported sonochemical kinetics of nonvolatile surfactants.

Introduction

Fluorine is the most electronegative of elements. Fluorochemicals (FCs), organics with the majority of their hydrogens replaced by fluorines, display unique properties as compared to their hydrocarbon analogs[1]. The C-F bond is the strongest among organics (> 110 kcal/mol), and low C-F bond polarizabilites gives them both hydrophobic and oleophobic character. Fluorination protects against oxidation and FC coatings provide water and oil resistance. However, these same fluorochemical properties make them environmentally persistent and recalcitrant towards most conventional water-treatment technologies[2,3], since they are inert towards common chemical and microbial treatment[4–6]. Sulfate radical[7–9], advanced reduction[10,11], and photolytic techniques[8,12,13] can degrade perfluorinated surfactants, most yielding shorter-chain FCs as products. Moriwaki et al.[4] reported that ultrasonic irradiation of aqueous perfluorochemical solutions may provide a practical alternative.

Acoustic cavitation, as driven by ultrasonic irradiation, can be utilized for the decomposition of aqueous chemical contaminants[15–18]. Application of ultrasound to aqueous solutions forms cavitation bubbles, which will undergo transient collapse events[5]. Quasi-adiabatic compression of transient bubbles generates average vapor temperatures near 5000 K[20,21] and much higher bubble vapor core temperatures that lead to sonoluminescence[6,7]. Water vapor readily pyrolyzes under the transient high temperatures producing O-atoms, hydroxyl radicals, and H-atoms[8]. Hot vapor colliding with the collapsing bubble wall generates interfacial temperatures of at least 800 K[8,9]. Chemicals preferentially partitioning to the bubble vapor will decompose via pyrolytic and combustion reactions[10]. Involatile surfactants that are difficult to oxidize, such as PFOS and PFOA, will pyrolytically decompose at the bubble-water interface[4].

Understanding the physical processes that control PFOX (X = S or A) degradation rates is key to optimization of their sonochemical kinetics. PFOX sonochemical degradation involves an initial, rate-determining ionic headgroup cleavage at the bubble-water interface followed by relatively quick mineralization of the fluorocarbon tail[11]. However, adsorption of PFOS and PFOA to the bubble-water interface, a physical process required before interfacial sonochemistry can occur, has yet to be investigated.

Henglein and Kormann[12] noted that hydroxyl radical scavenging activity increased with increasing organic chain length at cavitation bubble interfaces, while Fyrillas and Szeri made numerical calculations[13] of nonvolatile surfactant adsorption to an oscillating bubble interface. Their model calculations predicted a decrease in the maximum Gibbs surface excess, $\Gamma_{Max,Sono}$, as compared to the equilibrium max surface excess, $\Gamma_{Max,Eq}$, due to surface site limitations at bubble radial minimums and an increase in sonochemical surface activity, K_{Sono}, relative to equilibrium surface activity, K_{Eq}, due to high-velocity radial oscillations. Concentration-dependent sonochemical degradation kinetics of humic materials[14] and pesticides[15] have been empirically modeled by Langmuir-Hinshelwood kinetics, suggesting adsorption to the bubble-water interface is the initial step in their primary sonochemical decomposition mechanism and is limiting at high concentrations. Sostaric and Reisz[31,32] observed saturation of alkyl radical production during concentration-dependent sonolysis of alkyl sulfates and sulfonates. However, radical production from nonvolatile surfactants of various chain lengths did not correlate well with equilibrium Gibb's surface excess values, Γ_{Eq}. The lack of correlation was concluded to arise from relatively short acoustic bubble lifetimes (100s of μs) as compared to ionic surfactant equilibration times (> 1 ms). Tronson et. al.[16] observed that

Langmuir competitive adsorption modeling using equilibrium SDS surface excess values, Γ_{Eq}^{SDS}, did not fit trends expected from sonoluminescence data. Total acoustic bubble volume measurements as a function of alcohol conentration correlated well with Γ_{Eq}, however, Γ_{Eq} overestimated sonochemical ionic surfactant adsorption[17]. Sonochemical adsorption of nonvolatile (i.e., ionic) surfactants is not well described by equilibrium partitioning.

Here, we investigate sonochemical PFOS and PFOA adsorption to the bubble-water interface by determining absolute rates over 4 orders of magnitude of initial PFOX concentrations. Sonochemical effects on surface activity, K_{Sono}^{PFOX} vs. K_{Eq}^{PFOX}, are evaluated by modeling the concentration-dependent kinetics with the Langmuir-Hinshelwood formalism using an empirically determined V_{Max}^{-PFOX}, and comparing the results to equilibrium surface partitioning determined by surface tension measurements. Sonochemical PFOX surface activity determined here is compared to previously observed results.

Experimental Methods

Ammonium perfluorooctanoate (APFO) and sodium perfluorosulfonate (PFOS) were provided by the 3M Corporation. Ammonium acetate (> 99%) and methanol (HR-GC > 99.99%) were obtained from EMD Chemicals, Inc. Aqueous solutions were prepared with distilled and deionized water that was further purified using a MilliPore system (18.2 MΩ-cm resistivity).

Ultrasonic irradiation was performed at a frequency of 354 kHz and an applied power density of 250 W L^{-1} with an Allied Signal ELAC Nautik ultrasonic transducer. The average energy transferred to solution was 75%, as determined by calorimetry. The

reaction solution was contained in a 600 mL water-jacketed, glass reactor. The temperature was controlled with a Haake A80 refrigerated bath maintained at 10 ºC. All reactions were continuously sparged with argon for 30 minutes prior to and for the duration of the reaction. PFOS and PFOA were sonicated simultaneously over an initial concentration range of 20 nM to 200 μM. Higher concentrations were not tested as sonication caused the compounds to precipitate. Concentration vs. time profiles were fitted either to a single exponential decay for first-order kinetics, or linearly for zero-order kinetics.

Analysis of PFOA and PFOS was completed by HPLC-MS. The samples were placed into 750 μL polypropylene autosampler vials and sealed with a PTFE septum crimp cap. For reactions with intial concentrations greater than 250 ppb, serial dilutions to achieve a concentration ~ 50 ppb were completed prior to analysis. Aliquots (20 μL) were injected into an Agilent 1100 LC for separation on a Betasil C18 column (Thermo-Electron) of dimensions 2.1 mm ID, 100 mm length, and 5 μm particle size. A 2 mM aqueous ammonium acetate / methanol mobile phase at a flow rate of 0.75 mL min^{-1} was used with an initial composition of 70:30 water / methanol. Analytical procedures are detailed in previous reports[11]. The HPLC effluents were analyzed with an Agilent Ion Trap MS in the negative ion mode for the perfluorooctanesulfonate molecular ion (m/z = 499) and the decarboxylated perfluoroctanoate (m/z = 369). The nebulizer gas pressure was 40 PSI, while the drying gas flow rate and temperature were 9 L min^{-1} and 325 ºC, respectively. The capillary voltage was set at + 3500 V and the skimmer voltage was – 15 V. Quantification was completed by first producing a calibration curve using 8 concentrations between 1 ppb and 200 ppb fitted to a quadratic with X^{-1} weighting.

Surface tension measurements were made with a De Nouy tensiometer utilizing the standard ring method (ASTM D1331-89). The tensiometer was calibrated with a weight of known mass. Each sample was measured three times with the deviation between measurements less than 1%. The PFOS measurements were completed up to ~ 1 mM where the compound became insoluble. The curve was fitted to the surface pressure equation of state using Matlab to determine the partitioning coefficient and the maximum surface concentration.

Results

PFOX Concentration-Dependent Sonochemical Kinetics

Sonolysis of aqueous solutions containing both PFOS and PFOA were carried out over a range of initial concentrations from 20 nM to 200 μM (ν = 354 kHz, ρ_{PD} = 250 W L^{-1}, I = 6.4 W cm^{-2}). A plot of $[PFOS]_t/[PFOS]_i$ vs. time for a representative set of PFOS concentrations is shown in Figure 4.1a. At PFOS concentrations over the range of 20 nM to 14 μM, the observed kinetics are pseudo-first-order over four half-lives and are fitted to a single exponential decay. Previously reported results on PFOS and PFOA sonochemical decomposition completed at $[PFOS]_i \leq 20$ μM displayed a similar kinetic order[4,11]. At PFOS concentrations of 39 μM to 202 μM, the reaction kinetics are zero-order over the entire time-course. At an intermediate PFOS concentration of 30 μM, the data is fit to a quasi-exponential decay after the concentration dropped below 25 μM after 30 minutes of sonication. The transition from pseudo-first-order kinetics at low concentrations to zero-order kinetics at high concentrations is consistent with saturation kinetics. Initial PFOS sonochemical decomposition occurs pyrolytically at the bubble-water interface, therefore at high $[PFOS]_i$ the number of transiently cavitating bubble-water interfacial adsorption sites becomes saturated.

A qualitatively similar transition was observed for the sonolytic degradation of PFOA upon increasing the initial PFOA concentration. A plot of $[PFOA]_t/[PFOA]_i$ vs. time for a representative set of concentrations is shown in Figure 4.1b. At initial PFOA concentrations over the range of 24 nM to 6.5 μM, the reaction kinetics are pseudo first-order over at least four half-lives and are fitted to an exponential decay. At higher initial concentrations where $[PFOA]_i \geq 35$ μM, the reaction kinetics are zero-order over the entire time-course. At intermediate concentrations of 13.2, 16.6, and 30.5 μM, the reaction kinetics appear to be exponential after the first 30 minutes of reaction. The kinetic transition from pseudo-first-order to zero-order decay is similar to that observed for PFOS, and consistent with saturation kinetics

The observed kinetic parameters are given in Table 4.1. For low initial concentrations, $[PFOS]_i < 25$ μM and $[PFOS]_i < 13$ μM, the time-dependent plot was fitted to an exponential curve to determine the first-order rate constant, k_{app}^{-PFOX} (min^{-1}), and eq. 4.1 was used to determine the absolute rate.

$$\frac{d[PFOX]}{dt} = -k_{app}^{-PFOX}[PFOX] \tag{4.1}$$

For high initial concentrations, $[PFOX]_i > 40$ μM, the time-dependent plot was fitted to a linear curve with the slope, $k_{app}^{-PFOX'}$, taken to be the absolute degradation rate, eq. 4.2.

$$\frac{d[PFOX]}{dt} = -k_{app}^{-PFOX'} \tag{4.2}$$

For intermediate concentrations, the decay for the first 30 minutes was assumed to be linear and fit to eq. 4.2 and the decay after 30 minutes was fit to eq. 4.1. The overall degradation rate in Table 4.1 was taken as the temporal average of these two rates.

Equilibrium Partitioning to the Air-Water Interface

The Langmuir model describes adsorption to an interface. In the Langmuir model, the surface excess, Γ_{ex} , is a function of the equilibrium interface partitioning constant or surface activity, K_{eq} in L mol^{-1}, and the maximum surface concentration, Γ_{max} in mol m^{-2}. For example, equilibrium adsorption of PFOX to the air-water interface is modeled as shown in eq. 4.3.

$$\Gamma_{ex,eq}^{PFOX} = \Gamma_{Max,eq}^{PFOX} \frac{K_{eq}^{PFOX}[PFOX]}{1 + K_{eq}^{PFOX}[PFOX]} \tag{4.3}$$

The corresponding $\Gamma_{eq,ex}^{PFOX}$ and K_{eq}^{PFOX} values are determined from the dependence of surface tension on [PFOX], Figure 4.2, by least-squares fitting of the surface pressure to the Szyszkowski equation, eq. 4.4

$$\Pi = \gamma_0 - \gamma_{[PFOX]} = nRT\ \Gamma_{Max,eq}^{PFOX} \ln(1 + K_{eq}^{PFOX}[PFOX]) \tag{4.4}$$

where Π is the surface pressure in N m^{-1}, γ_0 = 0.072 N m^{-1} is the surface tension of pure water, and $\gamma_{[PFOX]}$ is the surface tension at [PFOX]. Maximum air-water interface concentrations of $\Gamma_{Max,eq}^{PFOA}$ = 4.5 x 10^{-6} mol m^{-2} and $\Gamma_{Max,eq}^{PFOS}$ = 5.1 x 10^{-6} mol m^{-2}, and equilibrium partitioning coefficients of K_{eq}^{PFOA} = 360 L mol^{-1} and K_{eq}^{PFOS} = 1970 L mol^{-1} are determined. The surface tension of solutions containing both PFOS and PFOA at equal concentrations was also measured and is plotted in Figure 4.2a. The stronger surfactant, PFOS, controls the surface tension as observed by the near overlap of the $\gamma_{[PFOS]}$ vs. [PFOS] curve and the $\gamma_{[PFOS]+[PFOA]}$ vs. [PFOS] + [PFOA] curve. Both the PFOS alone and [PFOS] + [PFOA] curves truncate between 1 to 2 mM, as the sodium salt of PFOS becomes insoluble in water. However, the agreement $\Gamma_{Max,eq}^{PFOX}$ and K_{eq}^{PFOX} values calculated here with previously determined values[35–38] shows that solubility limits

have minimal effect on the surface pressure fitting. Surface excess values vs. [PFOX] are plotted in Figure 4.2b; solid lines for individual PFOX curves and dashed lines for individual components of [PFOS] + [PFOA] curve. A competitive adsorption isotherm was used to plot the [PFOS] + [PFOA] surface excess values for each component. For example, eq. 4.5 was used for PFOA.

$$\Gamma_{ex,eq}^{PFOA} = \Gamma_{Max,eq}^{PFOA} \frac{K_{eq}^{PFOA}[PFOA]}{1 + K_{eq}^{PFOA}[PFOA] + K_{eq}^{PFOS}[PFOS]} \tag{4.5}$$

PFOS is observed to be the dominant surfactant in Figure 4.2b, as PFOA competition has little effect on the surface excess curve. In contrast, PFOA's surface excess curve under saturation conditions is shifted downward as PFOS outcompetes PFOA for air-water interface sites. The surface excess of PFOA under saturation conditions is decreased 7.2 times in the competition curve (dashed) as compared to the PFOA curve (solid).

Discussion

d[PFOX]/dt vs. $[PFOX]_i$ Sonochemical Kinetic Modeling

The transition from first-order to zero-order kinetics upon increasing the initial concentrations is consistent with saturation kinetics. Using the Langmuir-Hinshelwood approach[18] to model $[PFOX]_i$ sonochemical kinetics, the absolute rate is proportional to θ_{Sono}^{PFOX}, the fraction of total molecules adsorbed to the transiently cavitating bubble-water interface, eqs. 4.6 and 4.7

$$\theta_{Sono}^{PFOX} = \frac{K_{Sono}^{PFOX}[PFOX]}{1 + K_{Sono}^{PFOX}[PFOX]} \tag{4.6}$$

$$\frac{d[PFOX]}{dt} = -V_{Max}^{-PFOX}\theta_{Sono}^{PFOX} \tag{4.7}$$

where V_{Max}^{-PFOX} (M s^{-1}) is the maximum reaction rate when all the available bubble surface sorption sites are occupied.

The transition in kinetic regimes is consistent with Langmuir-Hinshelwood kinetic limits. At low PFOX concentration, when the surface is undersaturated and the observed kinetics are pseudo-first-order:

$$K_{Sono}^{PFOX}[PFOX] << 1 \tag{4.8}$$

$$\theta_{Sono}^{PFOX} = K_{Sono}^{PFOX}[PFOX] \tag{4.9}$$

$$\frac{d[PFOX]}{dt} = k_{app}^{-PFOX}[PFOX] = -V_{Max}^{-PFOX} K_{Sono}^{PFOX}[PFOX] \tag{4.10}$$

$$k_{app}^{-PFOX} = -V_{Max}^{-PFOX} K_{Sono}^{PFOX} \tag{4.11}$$

At intermediate concentration, there is a barrier to continued adsorption as the interfacial sites become increasingly populated, % levels:

$$\frac{d[PFOX]}{dt} = -V_{Max}^{-PFOX} \frac{K_{Sono}^{PFOX}[PFOX]}{1 + K_{Sono}^{PFOX}[PFOX]} \tag{4.12}$$

At high concentration, all of the surface sites are occupied and the maximum absolute rate is achieved:

$$K_{Sono}^{PFOX}[PFOX] >> 1 \tag{4.13}$$

$$\frac{d[PFOX]}{dt} = -V_{Max}^{-PFOX} \tag{4.14}$$

Thus, at low and intermediate concentration the kinetics are controlled by the fraction of the total PFOX molecules, which are absorbed to the bubble-water interface, as given by the Langmuir isotherm (eq. 4.6). At high concentration, the bubble-water interface is saturated with PFOX molecules and the rate is limited by the intrinsic chemical reaction rate (e.g., PFOX pyrolysis)[40–45].

Figures 4.3a and b plot the PFOX absolute degradation rate vs. $[PFOX]_i$ in linear-linear and log-log format, respectively; values from Table 4.1. Over the initial concentration range, 20 nM < $[PFOX]_i$ < 2000 nM, k_{app}^{-PFOX} (eq. 1) are constant; k_{app}^{-PFOA} = 0.047 min^{-1}, k_{app}^{-PFOS} = 0.028 min^{-1}, and k_{app}^{-PFOA} = 1.68 k_{app}^{-PFOS}. This indicates that the surface is undersaturated and the observed increase in absolute rate is due to the increasing θ_{Sono}^{PFOX}. However, at similar bulk concentrations, PFOS is expected to have the greater equilibrium activity at the bubble-water interface even though the maximum interfacial concentrations are similar, $\Gamma_{\max}^{PFOA} = 1.1\,\Gamma_{\max}^{PFOS}$ because PFOS has a larger partitioning coefficient, $K_{eq}^{PFOS} = 5.5\ K_{eq}^{PFOA}$. Thus the theoretical sonochemical degradation rate for PFOA is greater than that for PFOS or $V_{Max,Theo}^{-PFOA} > V_{Max,Theo}^{-PFOS}$, and if $\theta_{Sono}^{PFOS} > \theta_{Sono}^{PFOA}$ then $V_{Max,Theo}^{-PFOA} / V_{Max,Theo}^{-PFOS} > \theta_{Sono}^{PFOS} / \theta_{Sono}^{PFOA}$. Given that $k_{app}^{-PFOA} = 1.68\ k_{app}^{-PFOS}$ (eq. 11) and $K_{eq}^{PFOS} / K_{eq}^{PFOA} = 5.5$, the theoretical ratio $V_{Max,Theo}^{-PFOA} / V_{Max,Theo}^{-PFOS}$ is determined to be 9.3 under current ultrasonic conditions.

At initial concentrations over the range of 13 μM < $[PFOX]_i$ < 150 μM, PFOS and PFOA absolute rates are observed to saturate at $V_{Max,App}^{-PFOA}$ = 240 ± 60 nM min^{-1} and $V_{Max,App}^{-PFOS}$ = 230 ± 60 nM min^{-1}, confirming that the bubble-water interface is saturated. Convergence of $V_{Max,App}^{-PFOA}$ and $V_{Max,App}^{-PFOS}$ is at variance with relative kinetics at low concentrations. Under saturation conditions, PFOS as the stronger surfactant should out-compete PFOA for bubble surface sites and thus is able to compensate for the difference in the theoretical maximum pyrolytic rate constants causing the apparent rates to converge. This is consistent with equilibrium partitioning where PFOS competition

decreased the PFOA surface excess by a factor of 7.2, Fig. 4.2b. If PFOA were to be sonolytically degraded in the absence of PFOS, it would be expected to have a maximum degradation rate approximately 9.3 times greater than the experimentally observed rate or $V_{Max}^{-PFOA} = 2230 \pm 560$ nM. The determined V_{Max}^{-PFOX} values, low concentration k_{app}^{-PFOX}, and eq. 11 are used to calculate K_{Sono}^{PFOX} values of $K_{Sono}^{PFOS} = 121{,}000$ M^{-1} and $K_{Sono}^{PFOA} = 28{,}500$ M^{-1}. Both values are greater than equilibrium air-water interface partitioning values, yielding relative sonochemical to equilibrium surface activities of $K_{Sono}^{PFOS} / K_{Eq}^{PFOS} = 60$ and $K_{Sono}^{PFOA} / K_{Eq}^{PFOA} = 80$, Table 4.2.

The absolute PFOS degradation rates are modeled using the competitive Langmuir-Hinshelwood model, eq. 4.15, as shown in Figure 4.4, where V_{Max}^{-PFOS} is set to the empirically determined value $V_{Max,app}^{-PFOS} =$ 230 nM min^{-1} and K_{Sono}^{PFOS} is set equal to K_{Eq}^{PFOS} (black line), $10 \times K_{Eq}^{PFOS}$ (blue line), and $100 \times K_{Eq}^{PFOS}$ (red line); K_{Eq}^{PFOA} was adjusted accordingly.

$$\frac{d[PFOS]}{dt} = -V_{Max}^{-PFOS} \frac{K_{Sono}^{PFOS}[PFOS]}{1 + K_{Sono}^{PFOS}[PFOS] + K_{Sono}^{PFOA}[PFOA]} \tag{4.15}$$

The primary plots of Figure 4.4 are in log-log format while the inset is in linear-linear format. The best fit to the experimental data (black dots) is obtained when $K_{Sono}^{PFOS} = 100 \times K_{Eq}^{PFOS}$. PFOA surface competition had little effect on the fit as the non-competitive LH model yields a similar result. Altering V_{Max}^{-PFOS} rather than K_{Sono}^{PFOS} does not improve the fitting of the LH model to the experimental data.

Applying the Langmuir-Hinshelwood formalism to PFOA sonochemical kinetics is slightly more difficult since it is the weaker surfactant and competitive adsorption will

have a more prominent effect, Figure 4.2. In Figure 4.5a, the absolute PFOA degradation rate vs. initial PFOA concentration is modeled using the competitive LH formalism, eq. 16, with V_{Max}^{-PFOA} set to the empirically determined 240 nM min^{-1} and K_{Sono}^{PFOA} set equal to K_{Eq}^{PFOA}(black line), 10 × K_{Eq}^{PFOA}(blue line), and 100 × K_{Eq}^{PFOA}(red line); K_{Eq}^{PFOS} was adjusted accordingly.

$$\frac{d[PFOA]}{dt} = -V_{Max}^{-PFOA} \frac{K_{Sono}^{PFOA}[PFOA]}{1 + K_{Sono}^{PFOA}[PFOA] + K_{Sono}^{PFOS}[PFOS]} \tag{4.16}$$

The model calculations underestimate the experimental data by at least an order of magnitude in both the surface-saturated and undersaturated regimes. In Fig. 4.5b, V_{Max}^{-PFOA} is set to 2230 nM min^{-1}, as calculated using the relationship $V_{Max,Theo}^{-PFOA}$ / $V_{Max,Theo}^{-PFOA}$ = 9.3 to account for PFOS outcompeting PFOA for bubble interface adsorption sites. When $K_{Sono}^{PFOA} = 100 \times K_{Eq}^{PFOA}$, the best qualitative fit to the experimental data is obtained. d[PFOA]/dt vs. $[PFOA]_i$ fits for noncompetitive LH models are provided in the supporting information document. With V_{Max}^{-PFOA} = 240 nM min^{-1}, $K_{Sono}^{PFOA} = 1000 \times K_{Eq}^{PFOA}$, a good data fit is obtained while at V_{Max}^{-PFOA} = 2230 nM min^{-1}; none of the models result in a good fit to the data.

As $[PFOX]_i$ increases to greater than 200 μM, d[PFOX]/dt increases substantially to > 1000 nM min^{-1}, at variance with the LH kinetic model. Previous reports on ionic surfactant sonochemistry provide insight into this phenomenon. Ashokkumar et al.[19] observed that upon increasing aqueous sodium dodecyl sulfate (SDS) concentration, sonoluminescence (SL) increased, reaching a maximum at [SDS] = 1 mM. The increase in SL was attributed to SDS accumulation and thus build-up of charge on the bubble surface. Electrostatic repulsion between charged bubbles reduced bubble clustering,

leading to a greater number of more intense SL active bubble events. Total bubble volume was reported to decrease as bulk [SDS] was increased, with a 50% reduction in total bubble volume at [SDS] = 100 μM[20] suggesting a reduction in bubble coalescence. Increasing [SDS] led to a decrease in broadband acoustic emission, even though total acoustic emission increased[21], suggesting a transition to a greater number of more intense bubble collapse events[22] due to reduction in bubble-bubble clustering and coalescence. As anionic surfactants, PFOS and PFOA would be expected to have a similar effect on bubble-bubble interactions as SDS. The increase in PFOX absolute degradation rate occurs at $[PFOX]_i > 100$ μM , consistent with SDS concentrations where SL, total bubble volume, and acoustic emission effects are observed to take affect. Reduction in bubble-bubble coalescence and clustering leading to a greater number of more intense bubble collapse events would result in a greater number of bubble interface face adsorption sites and consequently an increase in PFOX sonochemical degradation kinetics.

Non-Equilibrium Bubble Surface Activity

Optimized fitting of the experimental kinetic data as a function of [PFOX] to the LH model gives $K_{Sono}^{PFOS} = 60\ K_{Eq}^{PFOS}$ and $K_{Sono}^{PFOA} = 80\ K_{Eq}^{PFOA}$. Data from two previous reports, which are fit to LH kinetics, is presented in Table 4.2. Concentration-dependent alkyl radical production for sodium dodecyl sulfate (SDS) and sodium octyl sulfate (SOS) from the work of Sostaric and Reisz[31] was fit to the LH model using an empirically determined maximum rate of alkyl radical production. For both compounds, K_{Sono} appears to be greater than K_{Eq}. The relative difference between K_{Sono} and K_{Eq} was greater for the weaker surfactant: $K_{Sono}^{SDS} = 12.5\ K_{Eq}^{SDS}$ vs. $K_{Sono}^{SOS} = 410\, K_{Eq}^{SOS}$. This trend is expected to hold for sodium pentyl sulfonate (SPSo), a weaker surfactant than SOS,

which had a similar sonochemical surface activity to SOS and SDS. Kim and Jung[29] modeled sonochemical degradation of humic acids (anionic, surface-active, natural organic matter) with LH kinetics and their results give values of $K_{Sono} > K_{Eq}$ as well. The humic acid degradation kinetics gave the greatest relative surface activity difference, $K_{Sono}^{Humic} = 3400\, K_{Eq}^{Humic}$; most likely due to the very high applied acoustic power density, 14,000 W L^{-1}.

Greater sonochemical surface activity over that of the predicted equilibrium surface activity was predicted by the calcuations of Fryllis and Szeri[13]. Their work argues that high-velocity bubble oscillations should increase the transport of surfactants to a lightly populated surface. Their conclusions are in qualitative agreement with the work of Eller and Flynn[23] on rectified diffusion. Under their 'high frequency approximation', which is valid for f > 20 kHz, diffusion can be assumed to be a slow process as compared to the radial motion of acoustic bubbles. For example, the sonochemical surface activity can be broken in the ratio of the rates of adsorption to and desorption from the interface: $K_{Sono} = \frac{k_{ads}}{k_{des}}$. Thus an increase in k_{ads} or a decrease in k_{des} will result in an increase in K_{Sono}. It is much easier to rationalize an increase in k_{ads}. For a lightly populated surface $k_{ads} = k_{dif}$ and processes such as high-velocity bubble oscillations or acoustic microstreaming may enhance diffusion to the bubble interface. A rough, yet insightful example will be presented to further this point.

A transiently cavitating bubble will expand from its average initial radius, R_0, to its max radius, R_{max}, over a period of 0.5f, where f is the ultrasonic frequency[5]. R_{max} (μm) can be calculated using the equation:

$$R_{\max}(\mu m) = (3\ x\ 10^6 / f)(P_a - 1)(P_a)^{-1/2}[1 + 2(P_a - 1)/3]^{1/3} \qquad (4.17)$$

where P_a is the acoustic pressure ($P_a = (2\ \rho\ C_L I_A)^{1/2} / 101325$ bar), ρ is the density of water (1000 kg m^{-3}), C_L is the speed of sound in water (1500 m s^{-1}), and I_A is the acoustic intensity (51000 W m^{-2} at a calorimetric power of 120 watts over a transducer area of 23.5 cm^2). Assuming a monotonic distribution of bubbles[24], R_0 can be estimated as the average of $R_{max}/2.5$, which is the dynamic limit for transient cavitation, and R_B, which is Blake's radius of bubble dissolution[5]. Since $R_B << R_{max}/2.5$ the value of R_0 is roughly $R_{max}/5$. Sonochemical parameters of 354 kHz and 120 watts correspond to R_{max} = 18 μm and $R_{max}/5$ = 3.6 μm. Thus, a point on the bubble surface travels a radial distance of 14.4 μm over the rarefaction period of 1.4 μs and assuming a constant radial velocity, a point at the bubble surface will travel at 10 m s^{-1} during expansion under present sonochemical conditions. If we assume a diffusion constant of 10^{-5} cm^2 s^{-1} or 10^{-3} μm^2 μs^{-1} for PFOS and PFOA, over a period of 1.4 μs a single molecule is expected to travel around 35 nm, which is much less than the bubble radial motion of 14.4 μm over the same period.

The differential volume between the average initial bubble, R_0 = 3.6 μm, and a bubble at its maximum radius, R_{max} = 18 μm, is $V_{diff} = (4/3)\ \pi\ (18^3 - 3.6^3)$ = 24200 μm^3. Using the high-frequency assumption that the rate of diffusion is significantly less than the rate of radial expansion, then all of the PFOS or PFOA molecules contained in the initial volume would be packed into a sheath of 35 nm in radius around the maximal bubble volume, $V_{sheath} = (4/3)\ \pi\ (18.035^3 - 18^3)$ = 143 μm^3. The ratio of the initial differential bubble volume to the bubble sheath volume, V_{diff}/V_{sheath} = 170. This suggests that the sonochemically induced increase in PFOS and PFOA surface activity may be partially due to high-velocity bubble oscillations enhancing the diffusion of the fluorochemicals to

the bubble-water. Other effects such as acoustic microstreaming[24] may also be responsible for enhanced diffusion to the bubble interface and thus the sonochemical surface activity

The results here are seemingly at variance with recent work by Tronson et al.[33] and Sunartio et al.[34] which concluded that the Gibb's surface excess was not attained for non-volatile surfactants. Fyrillas and Szeri[28] predicted that high-velocity bubble oscillations would reduce the maximal surfactant bubble surface population. This is consistent with conclusions that relatively short acoustic bubble lifetimes (~ 100 μs), as compared to ionic surfactant equilibration times (> 1 ms), led to the Gibb's surface excess not being attained during ultrasonic irradiation. Examples of possible nonequilibrium sonochemical PFOS surface activites, K^{PFOS}, and possible nonequilibrium sonochemical max surface excesses, Γ_{Max}^{PFOS}, and their affects on the surface excess population, Γ_{ex}^{PFOS} (eq. 3), are presented in Figure 4.6. Variations in Γ_{Max}^{PFOS} lead to a vertical shift in the Γ_{ex}^{PFOS} vs. [PFOS] curve, with the expected sonochemical effect to be a decrease in Γ_{Max}^{PFOS} and thus an overall, concentration-independent decrease in Γ_{ex}^{PFOS}. Variations in K^{PFOS} lead to a horizontal shift in the Γ_{ex}^{PFOS} vs. [PFOS] curve. The experimental results presented here suggest an increase in K^{PFOS} and thus a shift in the direction of the ordinate. If a decrease in Γ_{Max}^{PFOS} and an increase in K^{PFOS} occur upon moving from equilibrium air-water interface partitioning to a sonochemical air-water interface partitioning, then under surface saturation conditions a decrease Γ_{ex}^{PFOS} would still be predicted. Therefore, the experimental results presented suggesting a sonochemical increase in surface activity, $K_{Sono} > K_{Eq}$, are not necessarily at variance with previous

results suggesting the Gibb's surface excess was not attained for nonvolatile solutes. For example, in Figure 4.6c, simultaneous variations in both Γ_{Max}^{PFOS} and K^{PFOS} have been plotted. Decreasing Γ_{Max}^{PFOS} by a factor of ten also reduces Γ_{ex}^{PFOS} under lightly populated conditions by a factor of 10 (green line). Increasing K^{PFOS} by a factor of 10 (blue line) brings Γ_{ex}^{PFOS} to the equilibrium level (black line) for undersaturation conditons. Furthermore, when Γ_{Max}^{PFOS} is decreased by a factor of 10 and K^{PFOS} is increased by a factor of 100 (red line), the Γ_{ex}^{PFOS} then exceeds the predicted equilibrium adsorption limit for lightly populated conditions and is still below predicted equilibrium adsorption for saturation conditions.

Conclusions

The sonochemical degradation kinetics of PFOS and PFOA have been studied over the concentration range of 20 nM < $[PFOX]_I$ < 200 μM. The kinetics are fit to the Langmuir-Hinshelwood model using experimental rate maximums of V_{Max}^{-PFOA} = 2230 ± 560 nM min^{-1} and V_{Max}^{-PFOS} = 230 ± 60 nM min^{-1}. The corresponding sonochemical bubble surface activities for PFOS and PFOA are determined to be K_{Sono}^{PFOS} = 120,000 M^{-1} and K_{Sono}^{PFOA} = 28,500 M^{-1}, respectively. Competitive bubble surface adsorption is factored into the LH model in order to accurately model the kinetics of PFOA under saturation conditions. The sonochemical surface activities, K_{Sono}^{PFOX}, are 50 to 100 times greater than the predicted equilibrium air-water interfacial activities, K_{Eq}^{PFOX}, as determined via concentration-dependent surface tension measurements. The apparent enhancements in bubble surface activities has positive implications for the application of ultrasonic irradation as a treatment technology for dilute, < 1 μM, aqueous solutions of PFOS and

PFOA. At low concentrations, the efficacy of conventional chemical treatment methods is greatly reduced due to concentration effects. These results will also have implications for the sonochemical destruction of other pollutants where adsorption to the transiently cavitating bubble interface is expected to partially mediate absolute degradation rates.

Figures

Figure 4.1. PFOX sonochemical degradation initial concentration dependence. (358 kHz, 250 W L^{-1}, Ar, 10 ^{o}C). A) $[PFOS]_t$ / $[PFOS]_i$ vs. time in minutes. $[PFOS]_i$ = (●) 20 nM, (○) 14 μM, (▼) 30 μM, (▽) 39 μM, (■) 67 μM, and (□) 114 μM. B) $[PFOA]_t$ / $[PFOA]_i$ vs. Time (in minutes). $[PFOA]_i$ = (●) 20 nM, (○) 6.5 μM, (▼) 13.2 μM, (▽) 16.6 μM, (■) 30.5 μM, (□) 105 μM, and (◆) 220 μM

A

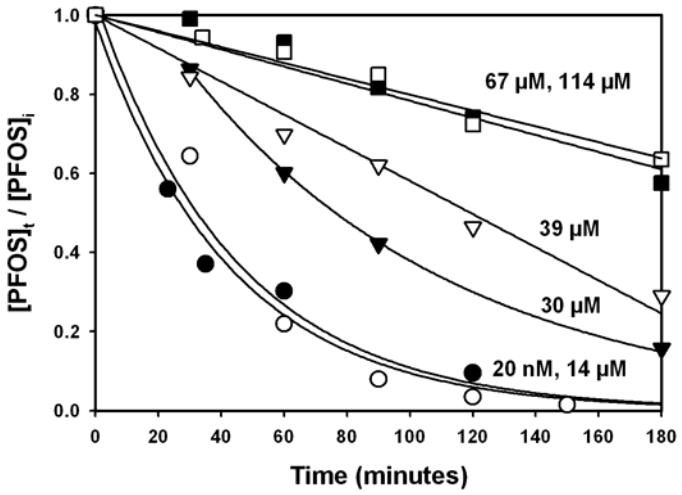

B

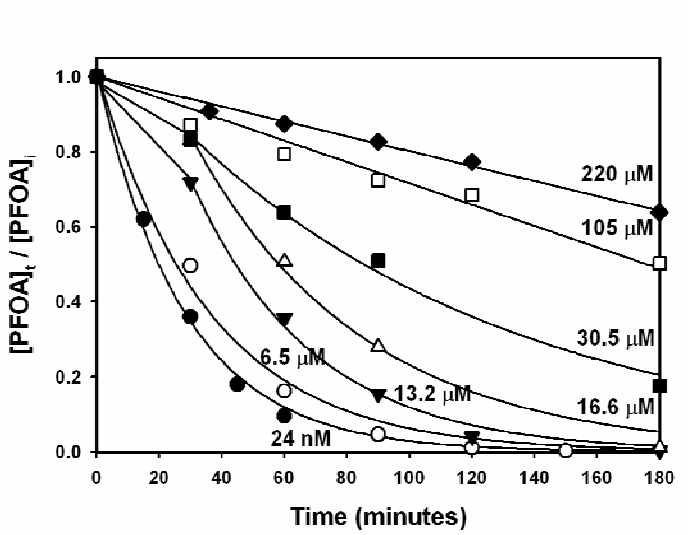

Figure 4.2. Equilibrium PFOX air-water interface partitioning. A) Plot of surface tension vs. aqueous PFOS and/or PFOA concentration. (●) PFOA, (●) PFOS, and (▼) PFOS & PFOA. B) Plot of surface excess vs. aqueous PFOS and/or PFOA concentration. (○) PFOA noncompetitive, (○) PFOS noncompetitive, (--) PFOA competitive, and (--) PFOS competitive

A

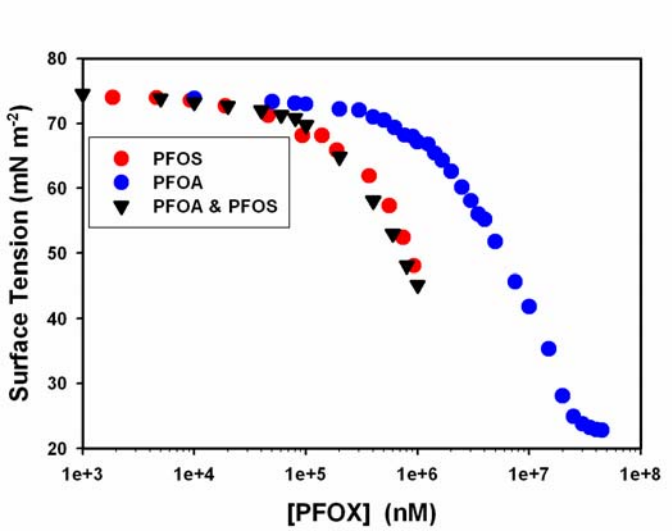

B

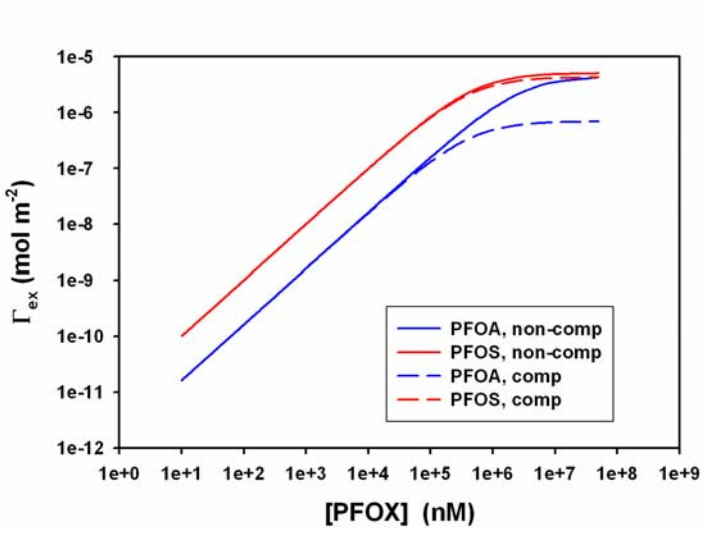

Figure 4.3. PFOX sonochemical degradation rate initial concentration dependence. PFOS and PFOA were simultaneously degraded under ultrasonic conditions: 358 kHz, 250 W L^{-1}, 10 ^{o}C, and argon. (○) PFOA and (○) PFOS. A) Linear-linear plot with the inset truncating off the final three data points. B) Log-log plot

A

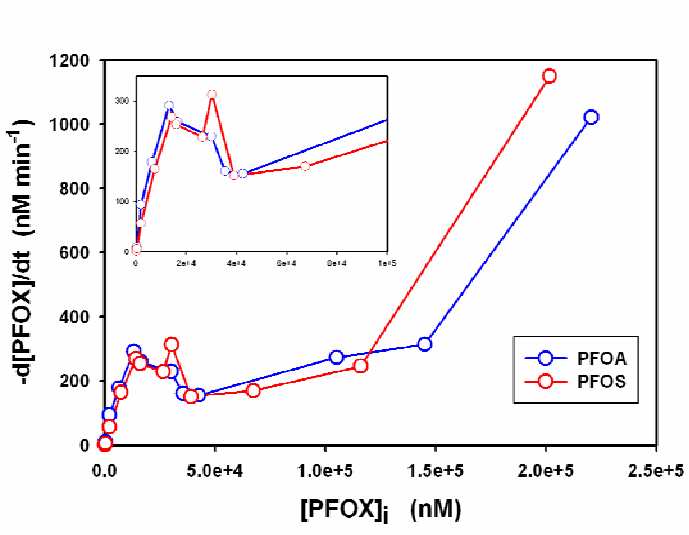

B

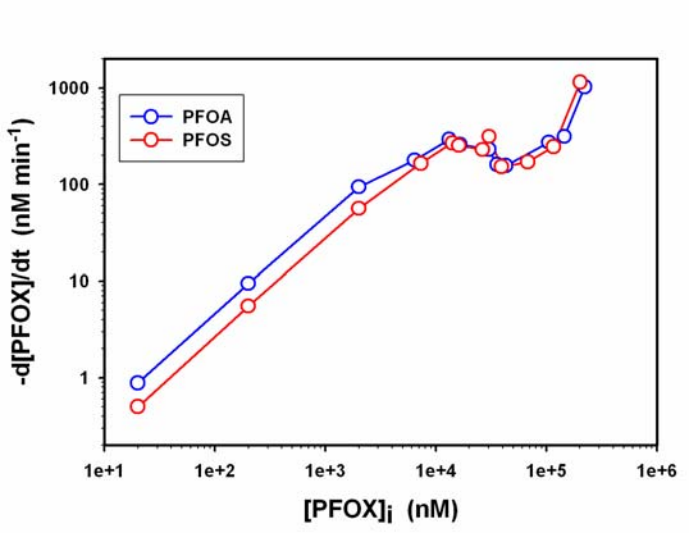

Figure 4.4. Kinetic modeling of PFOS sonolysis concentration-dependent kinetics. – [PFOS]/dt vs. $[PFOX]_i$ fitted by competitive Langmuir-Hinshelwood model, eq. 4.15: $V_{Max,app}^{-PFOS} =$ 230 nM min^{-1}. (●) Experimental, (—) $K_{Sono}^{PFOS} = K_{Eq}^{PFOS}$, (—) $K_{Sono}^{PFOS} = 10 \times K_{Eq}^{PFOS}$ and (—) $K_{Sono}^{PFOS} = 100 \times K_{Eq}^{PFOS}$

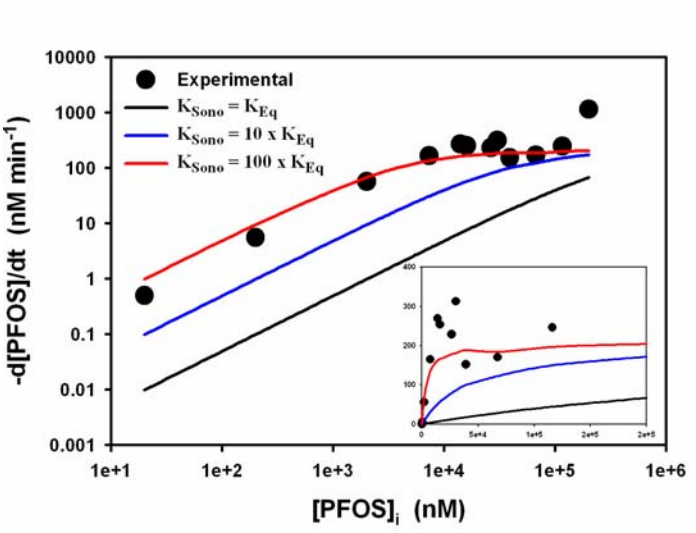

Figure 4.5. Kinetic modeling of PFOA sonolysis concentration-dependent kinetics. – [PFOA]/dt vs. $[PFOA]_i$ fitted by competitive Langmuir-Hinshelwood model (eq. 16): A) $V_{Max}^{-PFOA} =$ 240 nM min^{-1} and C) $V_{Max}^{-PFOA} =$ 2230 nM min^{-1}. (●) Experimental, **(—)** $K_{Sono}^{PFOA} = 100 \times K_{Eq}^{PFOA}$, **(—)** $K_{Sono}^{PFOA} = 100 \times K_{Eq}^{PFOA}$ and **(—)** $K_{Sono}^{PFOA} = 100 \times K_{Eq}^{PFOA}$

A

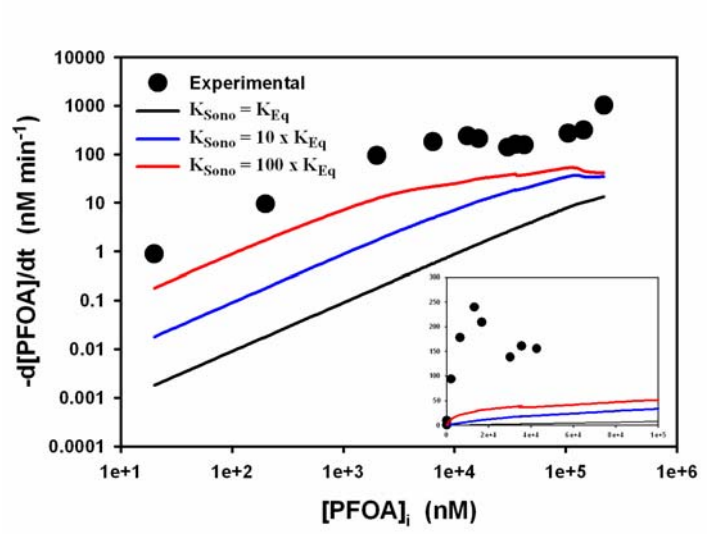

B

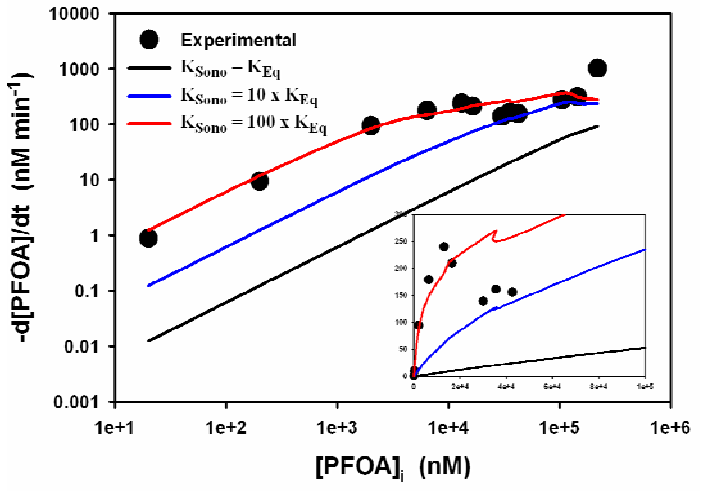

Figure 4.6. PFOS surface excess vs. PFOS bulk concentration (eq. 5): a) (○) Γ_{Max}^{PFOS}, (○) $10 \times \Gamma_{Max}^{PFOS}$, and (○) $0.1 \times \Gamma_{Max}^{PFOS}$, B) (○) K_{Eq}^{PFOS}, (○) $10 \times K_{Eq}^{PFOS}$, and (○) $0.1 \times K_{Eq}^{PFOS}$, and C) (○) Γ_{Max}^{PFOS} and K_{Eq}^{PFOS}, (○) $0.1 \times \Gamma_{Max}^{PFOS}$ and K_{Eq}^{PFOS}, (○) $0.1 \times \Gamma_{Max}^{PFOS}$ and $10 \times K_{Eq}^{PFOS}$, and (○) $0.1 \times \Gamma_{Max}^{PFOS}$ and $100 \times K_{Eq}^{PFOS}$

A

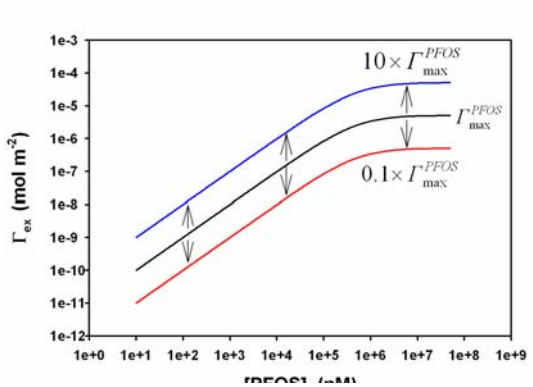

B

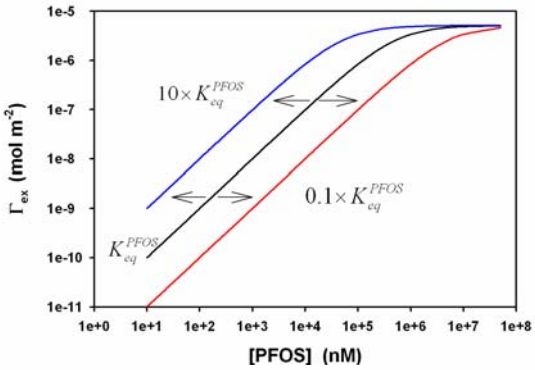

C

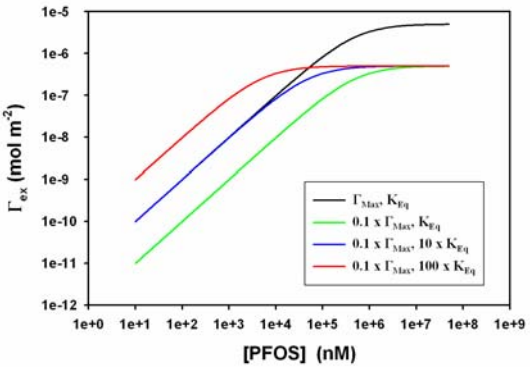

Tables

Table 4.1. Concentration-dependent PFOX sonochemical kinetics

[PFOA] (nM)	1st-Order (min^{-1})	0-Order (M min^{-1})	$\frac{-d[PFOA]}{dt}$ (M min^{-1})	[PFOS] (nM)	1st-Order (min^{-1})	0-Order (M min^{-1})	$\frac{-d[PFOS]}{dt}$ (M min^{-1})
20	0.044 ± 0.013		0.88	20	0.025 ± 0.005		0.5
200	0.047 ± 0.002		9.5	200	0.028 ± 0.006		5.5
2000	0.047 ± 0.005		94	2000	0.028 ± 0.005		56
6400	0.028		180	7300	0.023		165
13100	0.026	51	292	14000	0.019		269
16500	0.0184	39	259	16000	0.019	10	254
30000	0.0088	65	230	26400	0.01	56	229
35500		161	161	30200	0.012	69	313
42500		156	156	39000		152	152
105000		273	273	67300		170	170
145000		314	314	116000		250	250
221000		1022	1022	202000		1150	1150

Table 4.2. Sonochemical vs. equilibrium surface activity

	Frequency (kHz)	Applied Power Density (W L^{-1})	$\Gamma_{eq,\max}$ (mol m^{-2})	K_{eq} (M^{-1})	$V_{sono,\max}$	K_{Sono} (M^{-1})	$\frac{K_{Sono}}{K_{Eq}}$	Ref.
PFOS	354	250	5.1e-6	1,970	230 nM min^{-1}	121,000	60	this work
PFOA	354	250	4.5e-6	360	1660 nM min^{-1}	28,500	80	this work
SDS	47		6.9e-6[25]	400[25]	1 μM min^{-1}	5,000	12.5	[26]
SOS	47		6.4e-6[25]	22[25]	1.4 μM min^{-1}	8,000	410	[26]
Humic	20	14,000	4.6e-6[27]	1,180[27]		4e6	3,400	[29]

References

(1) 3M Company. *The Science of Organic Fluorochemistry*; Docket AR226-0547; Office of Pollution Prevention and Toxics, U.S. Environmental Protection Agency: Washington, D.C., 1999; p. 12.

(2) 3M Company. *Sulfonated perfluorochemicals in the environment: Sources, dispersion, fate and effects*; Docket AR226-0620; Office of Pollution Prevention & Toxics, U.S. Environmental Protection Agency: Washington, D.C., 2000; p. 51.

(3) 3M Company. *Removal of PFOA with Granular Activated Carbon: 3M Wastewater Treatment System Monitoring*; Docket AR226-1699; Office of Pollution Prevention & Toxics, U.S. Environmental Protection Agency: Washington, D.C., 2004; p. 5.

(4) Key, B. D.; Howell, R. D.; Criddle, C. S. *Environ. Sci. Technol.* **1998**, *32*, 2283.

(5) Schultz, M. M.; Higgins, C. P.; Huset, C. A.; Luthy, R. G.; Barofsky, D. F.; Field, J. A. *Environ. Sci. Technol.* **2006**, *40*, 7350.

(6) Schroder, H. F.; Meesters, R. J. W. *J. Chromatogr. A* **2005**, *1082*, 110.

(7) Hori, H.; Yamamoto, A.; Hayakawa, E.; Taniyasu, S.; Yamashita, N.; Kutsuna, S.; Kiatagawa, H.; Arakawa, R. *Environ. Sci. Technol.* **2005**, *39*, 2383.

(8) Chen, J.; Zhang, P. *Water Sci. Technol.* **2006**, *54*.

(9) Hori, H.; Hayakawa, E.; Einaga, H.; Kutsuna, S.; Koike, K.; Ibusuki, T.; Kiatagawa, H.; Arakawa, R. *Environ. Sci. Technol.* **2004**, *38*, 6118.

(10) Hori, H.; Nagaoka, Y.; Yamamoto, A.; Sano, T.; Yamashita, N.; Taniyasu, S.; Kutsuna, S.; Osaka, I.; Arakawa, R. *Environ. Sci. Technol.* **2006**, *40*, 1049.

(11) Yamamoto, T.; Noma, Y.; Sakai, S. I.; Shibata, Y. *Environ. Sci. Technol.* **2007**, *41*, 5660.

(12) Hori, H.; Hayakawa, E.; Koike, K.; Einaga, H.; Ibusuki, T. *J. Mol. Catal. A—Chem.* **2004**, *211*, 35.

(13) Dillert, R.; Bahnemann, D.; Hidaka, H. *Chemosphere* **2007**, *67*, 785.

(14) Moriwaki, H.; Takagi, Y.; Tanaka, M.; Tsuruho, K.; Okitsu, K.; Maeda, Y. *Environ. Sci. Technol.* **2005**, *39*, 3388.

(15) Jennings, B. H.; Townsend, S. N. *J. Phys. Chem.* **1961**, *65*, 1574.

(16) Destaillats, H.; Hung, H. M.; Hoffmann, M. R. *Environ. Sci. Technol.* **2000**, *34*, 311.

(17) Kotronarou, A.; Mills, G.; Hoffmann, M. R. *J. Phys. Chem.* **1991**, *95*, 3630.

(18) Petrier, C.; David, B.; Laguian, S. *Chemosphere* **1996**, *32*, 1709.

(19) Brennen, C. E. *Cavitation and Bubble Dynamics*; Oxford University Press: New York, 1995.

(20) Didenko, Y. T.; McNamara, W. B.; Suslick, K. S. *J. Am. Chem. Soc.* **1999**, *121*, 5817.

(21) Ciawi, E.; Rae, J.; Ashokkumar, M.; Grieser, F. *J. Phys. Chem. B* **2006**, *110*, 13656.

(22) Ashokkumar, M.; Grieser, F. *J. Am. Chem. Soc.* **2005**, *127*, 5326.

(23) Eddingsaas, N. C.; Suslick, K. S. *J. Am. Chem. Soc.* **2007**, *129*, 3838.

(24) Leighton, T. G. *The Acoustic Bubble*; Academic Press: London, 1994.

(25) Hung, H. M.; Hoffmann, M. R. *J. Phys. Chem. A* **1999**, *103*, 2734.

(26) Vecitis, C. D.; Park, H.; Cheng, J.; Mader, B. M.; Hoffmann, M. R. *J. Phys. Chem. C* **2008**, *112*.

(27) Henglein, A.; Kormann, C. *Int. J. Radiat. Biol.* **1985**, *48*, 251.

(28) Fyrillas, M. M.; Szeri, A. J. *J. Fluid Mech.* **1996**, *311*, 361.

(29) Kim, I. K.; Jung, O. J. *Bull. Korean Chem. Soc.* **2001**, *22*, 1093.

(30) O'Shea, K. E.; Aguila, A.; Vinodgopal, K.; Kamat, P. V. *Res. Chem. Intermed.* **1998**, *24*, 695.

(31) Sostaric, J. Z.; Riesz, P. *J. Am. Chem. Soc.* **2001**, *123*, 11010.

(32) Sostaric, J. Z.; Riesz, P. *J. Phys. Chem. B* **2002**, *106*, 12537.

(33) Tronson, R.; Ashokkumar, M.; Grieser, F. *J. Phys. Chem. B* **2003**, *107*, 7307.

(34) Sunartio, D.; Ashokkumar, M.; Grieser, F. *J. Am. Chem. Soc.* **2007**, *129*, 6031.

(35) Lopez-Fontan, J. L.; Gonzalez-Perez, A.; Costa, J.; Ruso, J. M.; Prieto, G.; Schulz, P. C.; Sarmiento, M. *J. Colloid Interface Sci.* **2006**, *294*, 458.

(36) Lopez-Fontan, J. L.; Sarmiento, F.; Schulz, P. C. *Colloid Polym. Sci.* **2005**, *283*, 862.

(37) Simister, E. A.; Lee, E. M.; Lu, J. R.; Thomas, R. K.; Ottewill, R. H.; Rennie, A. R.; Penfold, J. *J. Chem. Soc.—Faraday Trans.* **1992**, *88*, 3033.

(38) Shinoda, K.; Hato, M.; Hayashi, T. *J. Phys. Chem.* **1972**, *76*, 909.

(39) Langmuir, I. *J. Am. Chem. Soc.* **1916**, *38*, 2221.

(40) Glockner, V.; Lunkwitz, K.; Prescher, D. *Tenside Surf. Det.* **1989**, *26*.

(41) Lines, D.; Sutcliffe, H. *J. Fluor. Chem.* **1984**, *25*, 505.

(42) Lazerte, J. D.; Hals, L. J.; Reid, T. S.; Smith, G. H. *J. Am. Chem. Soc.* **1953**, *75*, 4525.

(43) Hals, L. J.; Reid, T. S.; Smith, G. H. *J. Am. Chem. Soc.* **1951**, *73*, 4054.

(44) Krusic, P. J.; Marchione, A. A.; Roe, D. C. *J. Fluor. Chem.* **2005**, *126*, 1510.

(45) Krusic, P. J.; Roe, D. C. *Anal. Chem.* **2004**, *76*, 3800.

(46) Ashokkumar, M.; Hall, R.; Mulvaney, P.; Grieser, F. *J. Phys. Chem. B* **1997**, *101*, 10845.

(47) Lee, J.; Kentish, S. E.; Ashokkurnar, M. *J. Phys. Chem. B* **2005**, *109*, 5095.

(48) Ashokkumar, M.; Hodnett, M.; Zeqiri, B.; Grieser, F.; Price, G. J. *J. Am. Chem. Soc.* **2007**, *129*, 2250.

(49) Price, G. J.; Ashokkumar, M.; Hodnett, M.; Zequiri, B.; Grieser, F. *J. Phys. Chem. B* **2005**, *109*, 17799.

(50) Eller, A.; Flynn, H. G. *J. Acoust. Soc. Am.* **1965**, *37*, 493.

(51) Colussi, A. J.; Hung, H. M.; Hoffmann, M. R. *J. Phys. Chem. A* **1999**, *103*, 2696.

(52) Lunkenheimer, K.; Czichocki, G.; Hirte, R.; Barzyk, W. *Colloid Surf. A—Physicochem. Eng. Asp.* **1995**, *101*, 187.

(53) Tuckermann, R. *Atmos. Environ.* **2007**, *41*, 6265.